

Advection in chaotically time-dependent open flows

Z. Neufeld^{1,*} and T. Tél^{2,†}

¹*Department of Atomic Physics, Eötvös University, Puskin u. 5-7, H-1088 Budapest, Hungary*

²*Institute of Theoretical Physics, Eötvös University, Puskin u. 5-7, H-1088 Budapest, Hungary*

(Received 15 May 1997; revised manuscript received 30 September 1997)

The passive advection of tracer particles is considered in open two-dimensional incompressible flows with chaotic time dependence. As illustrative examples we investigate flows produced by chaotically moving ideal point vortices. The advection problem can be seen as a chaotic scattering process in a chaotically driven Hamiltonian system. Studying the motion of tracer ensembles, we present numerical evidence for the existence of a bounded chaotic set containing infinitely many aperiodic trajectories never leaving the mixing region of the flow. These ensembles converge to filamental patterns which, however, do not follow self-similar scaling. Nevertheless, they possess a fractal dimension after averaging over several finite-time realizations of the flow. We propose random maps as simple models of the phenomenon. [S1063-651X(98)11202-3]

PACS number(s): 47.10.+g, 05.45.+b, 47.15.Ki, 47.27.Cn

I. INTRODUCTION

The passive advection of tracer particles in two-dimensional incompressible flows is a chaotic phenomenon [1]. In such cases, the tracer dynamics turns out to be area preserving in the phase space which coincides with the plane of the flow and is thus directly observable. The advection in nonsteady flows is described by driven Hamiltonian dynamics. In the last decade, a comprehensive knowledge has accumulated in the case of strict *time periodicity* both for flows in closed containers [2–16] and for open flows with asymptotic simplicity [17–30], where the velocity field in the far up and downstream region is uniform. A unique feature of the latter sort of open flows is the pronounced and stable *fractal feature* associated with chaotic tracer dynamics. This is clearly measurable in laboratory experiments [31]. The central object governing the tracer dynamics is a nonattracting chaotic saddle [32] containing an infinite number of periodic and aperiodic bounded tracer orbits which never reach the far up or downstream region. The stable manifold represents the saddle's basin of attraction, and is a set of measure zero. The unstable manifold leads tracers which have approached the saddle in the far downstream region. Both the saddle and its stable and unstable manifolds are fractal objects. Since the asymptotic dynamics is simple, the tracer motion can be considered as a scattering process with all the characteristics of a periodically driven one-degree-of-freedom *chaotic scattering* [33].

Our aim in this paper is to study how this picture changes when the velocity field has a *chaotic* time dependence. We restrict ourselves to flows of asymptotic simplicity further on, which implies that the time dependence is relevant in a finite region of the plane only, in the so-called *mixing region*. Note that this does not mean at all that the flow would be turbulent here. In fact, we shall consider four-vortex problems as illustrative examples. Nevertheless, we do hope that

by understanding such cases, we come a step closer to the understanding of what passive transport looks like in flows exhibiting two-dimensional turbulence [34,35] in regimes of finite extents. In the language of point mechanics, such tracer motions correspond to chaotic scattering processes generated by chaotic temporal driving.

Studying the motion of tracer ensembles, we present numerical evidence for the existence of a *bounded chaotic set* containing trajectories never going out to the far upstream or downstream region. Although periodic orbits are atypical, an *infinite* number of aperiodic bounded orbits do belong to this set which seems thus to be a direct generalization of a chaotic saddle. Local Lyapunov exponents on it are found to be strictly positive.

Technically, it is easier to follow escape-time functions telling us how the time spent in the mixing region depends on the tracers' initial conditions (typically taken along a line segment). This distribution is found to be more irregular than in periodic flows, and is not consistent with the assumption of a single escape rate governing exponential decay statistics with a well-defined exponent. Nevertheless, a *range of instantaneous escape rates* can be found. The singularities of the escape-time function belong to the intersection of the line of initial conditions with the stable manifold of the bounded chaotic set. We shall call the stable manifold the *forward nonescaping foliation*.

Tracer droplets rapidly evolve an interwoven, *filamental* pattern along the unstable manifold of the bounded chaotic set. It will be called the *backward nonescaping foliation* because this is the set of infinite escape times in the time-reversed tracer dynamics. It cannot be distinguished by the naked eye from the fractal filaments of periodic flows. A closer observation, however, reveals that these foliations need not follow exact fractal scaling: the fractal dimension of such filaments might depend on the length scale of observation.

Since the chaotic time dependence of the flow is restricted to a finite region, its effect is similar to that of a bounded random noise. Thus in the weak sense of random averages the escape rate and the fractal dimension become well-

*Electronic address: neufeld@hercules.elte.hu

†Electronic address: tel@poe.elte.hu

defined quantities. More generally, clear asymptotic characteristics are obtained by averaging over several finite-time realizations of the chaotic flow.

As simple models of the phenomenon, we propose *open random maps* where some features are more pronounced than in the tracer dynamics. We show that the tracer dynamics has an asymptotic escape rate and a fractal dimension in the sense of random averages [36,37,10], provided that the driving dynamics has reached a stationary probability distribution. Even if this is fulfilled, the convergence towards the asymptotic values might be quite slow. The recently coined concept of *indecomposable continua* [29] seems to be an appropriate tool for describing the filamental patterns of the nonescaping foliations observed in chaotic flows.

The paper is organized as follows. In Sec. II we present four-vortex models generating the chaotic flows considered. Section III is devoted to the presentation of numerical results obtained for the tracer motion. In Sec. IV explanatory theoretical models are discussed, and the paper is closed by a short discussion (Sec. V).

II. THE FOUR-VORTEX DYNAMICS

The equations of motion of interacting ideal point vortices in incompressible two-dimensional flows can be written in the canonical form [38]

$$\Gamma_i \dot{x}_i = \frac{\partial H}{\partial y_i}, \quad \Gamma_i \dot{y}_i = -\frac{\partial H}{\partial x_i}, \quad i = 1, 2, \dots, N \quad (1)$$

where $\{x_i, y_i\}$ are the coordinates of vortex i of strength Γ_i . The Hamiltonian H appears in the form

$$H(\{x_i, y_i\}) = -\frac{1}{\pi} \sum_{i < j} \Gamma_i \Gamma_j \ln r_{i,j}, \quad (2)$$

with $r_{i,j}$ denoting the distance between vortices i and j .

Our aim now, as explained above, is to investigate advection in a velocity field produced by point vortices moving chaotically. It can be easily shown that the minimal number of vortices necessary for chaotic dynamics is four [2,38].

We are interested in advection in open flows where distant tracer particles can come close to the point-vortex system along a simple path, exhibit complicated motion around it, and then leave this system along a simple trajectory again (asymptotic simplicity). For such open flows the sum of the vortex strengths has to be zero ($\sum_{i=1}^4 \Gamma_i = 0$). In this case the streamlines far from the vortices are straight lines along which they can be approached. (For $\sum \Gamma_i \neq 0$ the streamlines far from the vortices are closed curves.)

Perhaps the simplest flow of asymptotic simplicity is generated by the so-called *leapfrogging* motion of two identical point-vortex pairs ($|\Gamma_i| = 1$, $i = 1, \dots, 4$) [26]. However, due to the special symmetry of the initial positions ($x_1 = x_4$, $x_2 = x_3$, $y_1 = -y_4$, and $y_2 = -y_3$, i.e., vortices 1 and 2 are mirror images of vortices 3 and 4), which is preserved by the dynamics, the motion of the vortices is nonchaotic, but periodic.

By considering another four-vortex system with the same set of vortex strengths $\Gamma_1 = \Gamma_2 = 1$, $\Gamma_3 = \Gamma_4 = -1$, but without restricting the initial conditions to a symmetric one, we

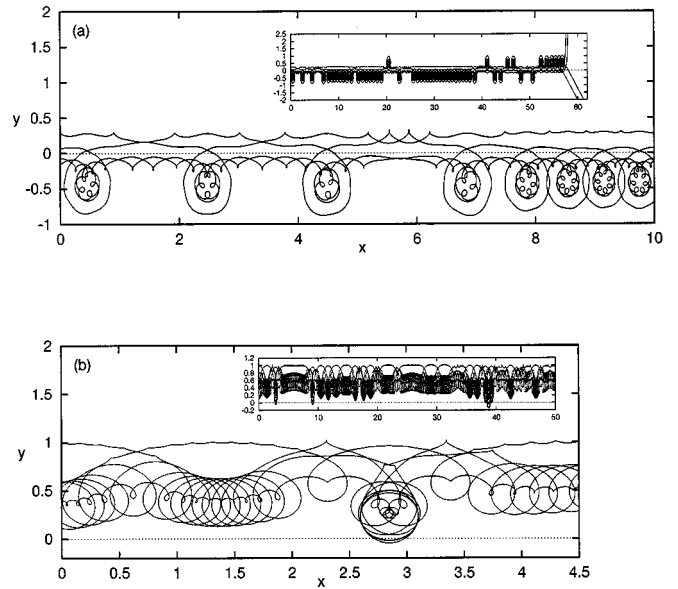


FIG. 1. Trajectories of four ideal vortices with vortex strengths (a) $\Gamma_1 = \Gamma_2 = 1$, $\Gamma_3 = \Gamma_4 = -1$; and (b) $\Gamma_1 = \Gamma_2 = \Gamma_3 = 1$, $\Gamma_4 = -3$. These dimensionless vortex strengths are measured in units of Γ , the dimensional vorticity of vortex 1. The initial positions of the vortices are (a) $x_1 = x_2 = x_3 = x_4 = 0$, $y_1 = 0.3$, $y_2 = 0.075$, $y_3 = -0.07$, $y_4 = -0.2$; and (b) $x_1 = x_2 = x_3 = x_4 = 0$, $y_1 = 0.1$, $y_2 = 0.6$, $y_3 = 1.0$, $y_4 = 0.4$. The length unit l is given in terms of the initial coordinates as $l = 5|y_4|$ and $l = |y_3|$ in cases (a) and (b), respectively. Trajectories are represented in dimensionless units. The time the system requires to pass through frames (a) and (b) is $t \approx 0.688$ and $t \approx 0.4$, respectively. Trajectories over longer times ($t \approx 4.9$ and $t \approx 4.2$) are shown in the insets. These dimensionless times are given in units of l^2/Γ . Note the asymptotic breakup of the four-vortex system in two vortex pairs in case (a).

obtain a locally chaotic and asymptotically steady open flow. The corresponding vortex trajectories are shown in Fig. 1(a). Unfortunately, this system is unstable in the sense that it can disintegrate into two vortex pairs moving away in different directions. In other words, the chaotic vortex motion itself is transient. This has been studied in great detail as a chaotic scattering process of vortex pairs [39]. The time on which the system breaks up in two pairs strongly depends, however, on the initial conditions. Thus one can choose appropriate initial conditions to make this time long enough for a convenient investigation of the chaotic advection.

One can even prevent this breakup by changing the vortex strengths to keep the vortices close to each other forever. The condition is that the system should not be decomposable into subsystems of zero resulting vortex strengths. The simplest case which satisfies this is $\Gamma_1 = \Gamma_2 = \Gamma_3 = 1$ and $\Gamma_4 = -3$ [Fig. 1(b)].

We shall consider these two chaotic four-vortex systems as illustrative examples of chaotically time-dependent open flows with asymptotic simplicity. Typical vortex trajectories are shown in Fig. 1. The common feature of both dynamics is that the four vortices move chaotically, do not depart from each other, and move together along a line. (The latter is true only for a finite period of time in the first example.) Thus the motion of the vortices can be seen as a superposition of a straight translating motion and a chaotic relative motion

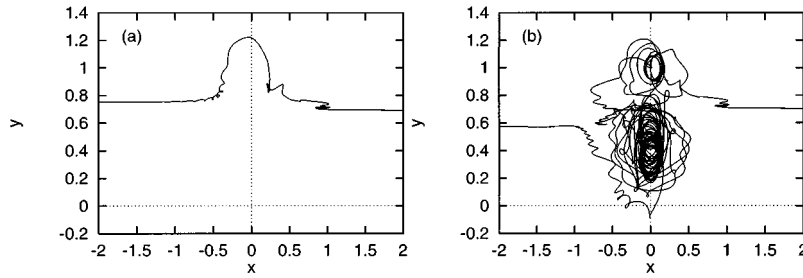


FIG. 2. Chaotic tracer trajectories in a chaotic flow. Trajectories are shown in a reference frame moving with the average vortex velocity $(\sum_{i=1}^4 \dot{x}_i)/4$. [The flow is generated by the vortex dynamics shown in Fig. 1(b).] The initial positions of the tracer particles are (a) $x=3.5$, $y=0.69$ and (b) $x=3.5$, $y=0.7$ and the time spent in the mixing region is 0.45 and 1.635, respectively.

which, in turn, produces a chaotic velocity field in a confined region. From the point of view of particle dynamics, this plays the role of the mixing region.

III. ADVECTION OF PASSIVE TRACERS

The dynamics of passively advected particles is determined by the underlying velocity field and is given by the superposition of the circular velocity flows of single vortices. The streamfunction ψ for a point-vortex system can be written in the form [38]

$$\psi(x,y,t) = - \sum_i \frac{\Gamma_i}{\pi} \ln r_i(t), \quad (3)$$

where $r_i(t)$ stands for the distance of point (x,y) from vortex i . The tracer equations of motion follow from the streamfunction ψ as

$$\dot{x} = \frac{\partial \psi(x,y,t)}{\partial y}, \quad \dot{y} = - \frac{\partial \psi(x,y,t)}{\partial x}. \quad (4)$$

Note the Hamiltonian character of the dynamical system (4).

The vortices generating the flow in our illustrative examples translate as a whole along a line. By introducing a comoving reference frame, we make the translation of the vortices disappear. In this *comoving* frame the velocity field ensures that particles are advected towards the mixing region and then leave it by moving away on asymptotically straight lines. Thus the condition for an open flow with asymptotic simplicity is fulfilled.

Similarly to periodic open flows, the advection of passive tracers is a chaotic scattering process. Typical trajectories of tracer particles in the comoving frame are shown in Fig. 2. As usual, the time spent in the mixing region, the escape time, as well as the trajectory itself are sensitively dependent on the initial coordinates of the tracers.

Lyapunov exponents measured along orbits of long escape times are clearly positive. The measurements have been carried out by starting a test particle with an initial condition close to that of a reference orbit (the initial distance is $\delta=10^{-5}$). The test particle departs from the reference orbit and whenever their distance becomes larger than a threshold value (10δ), we shift it back to a distance δ to the reference orbit, along the line connecting the test and reference particles. We counted the number n of such replacements up to time t (in fact, this number is proportional to the logarithm of

the total stretching rate) as a function of t . The average slope (see Fig. 3) gives an estimate of the Lyapunov exponent along the reference trajectory.

We can also investigate the evolution of an *ensemble* of tracer particles simulating the evolution of a droplet of dye injected into the mixing region. Snapshots taken at different times (Fig. 4) show that the ensemble tends to produce a complicated *filamental* structure characteristic to chaotic mixing and reminiscent to the ones observed in the case of periodic open flows. The latter has been identified with the unstable manifold of the chaotic saddle existing in the mixing region [22,23,26,27,29]. An important difference is, however, that in contrast to the periodic generation of identical lobes, here the emerging patterns continuously change their form and size due to the chaotic motion of the vortices driving the flow.

Using these tracer trajectories we can represent the escape time, the time spent in the mixing region, for each initial condition (Fig. 5). We are particularly interested in the singularities of the escape times, which mean trapping for a large, theoretically infinite, time in the mixing region. The latter was chosen for numerical purposes as a box centered initially at $x=y=0$ and moving with the average velocity of the vortex system $(\sum_{i=1}^4 \dot{x}_i)/4$. The size of this box was $l_x=l_y=4$ which is large enough to fulfill the condition that particles leaving it will never return to the mixing region again.

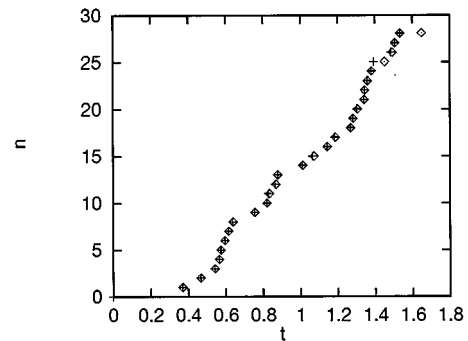


FIG. 3. Stretching number n vs time t measured (see text) along the trajectory shown in Fig. 2(b). Dots and diamonds represent results obtained for two different test particles started at different positions but at the same distance. The slope (~ 24) gives an estimate of the Lyapunov exponent ($24 \ln 10 \approx 55$). The saturation around $t=1.6$ is due to the escape from the mixing region.

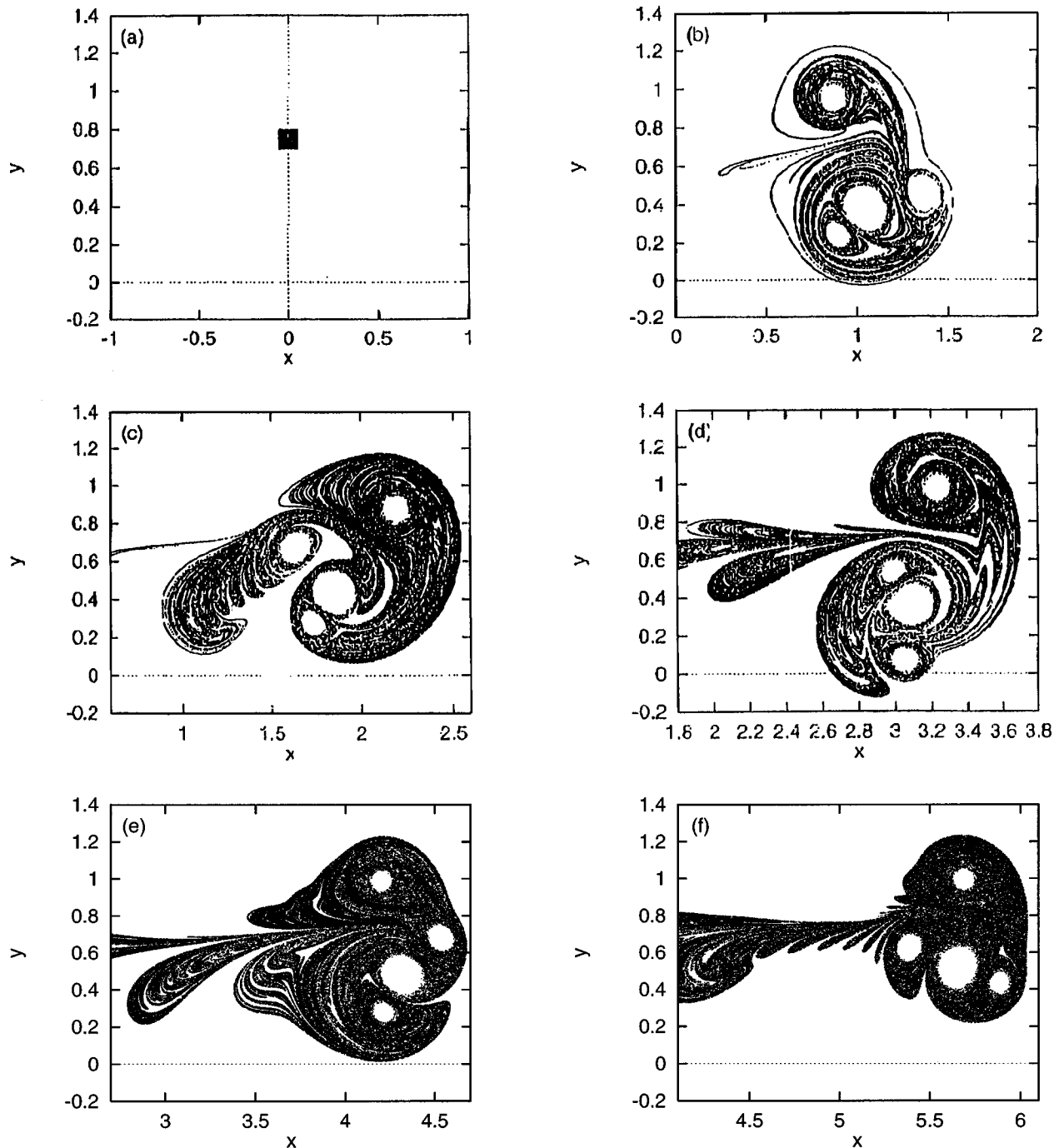


FIG. 4. Temporal evolution of an ensemble of 160.000 particles initially placed on a square grid of size 0.1 centered at $(0,0.75)$. Snapshots are taken at (a) $t=0$, (b) $t=0.1$, (c) $t=0.2$, (d) $t=0.3$, (e) $t=0.4$, and (f) $t=0.5$. After a time period of $t=0.5$, there are still 66.869 particles in frame (f). The vortex dynamics is the one shown in Fig. 1(b).

Figure 5(a) shows that there are two qualitatively different sets of initial conditions leading to long escape times. One of them is characterized by compact disk shaped structures situated around the vortices. The particles started in this set are trapped forever in these *vortex cores*, and their trajectories cannot be approached by particles coming from outside the cores. This kind of vortex cores is a generic feature of point-vortex dynamics, as was pointed out in different papers [34,35,15,16]. The motion of the tracers is regular around the chaotically moving vortex centers, being just a slaved chaotic motion with zero relative Lyapunov exponent. Since

particles cannot enter into these cores from outside, they are irrelevant for the chaotic scattering process we are interested in.

The other set of initial conditions with large escape times, on the contrary, has a complex filamental structure reminiscent of the fractal stable manifolds of the chaotic saddles observed in the case of time-periodic flows. The enlargements [for an example see Fig. 5(b)] illustrate that the complex patterns are present on all smaller scales. The motion of the particles on these filaments is restricted in the forward dynamics to the mixing region forever. Therefore we shall

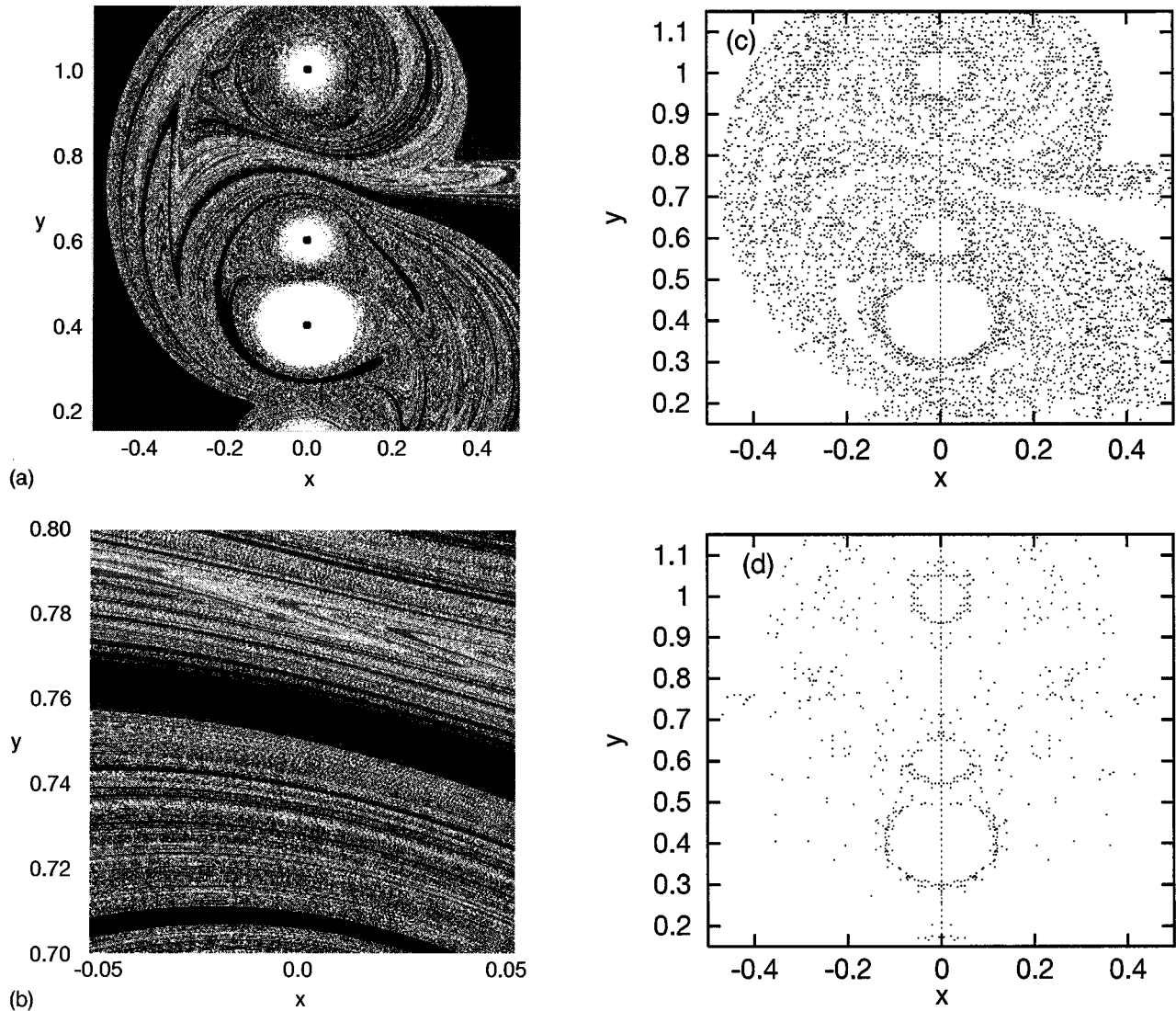


FIG. 5. The time spent in the mixing region, the escape time, represented on gray scale as a function of the initial position of 160.000 tracers distributed uniformly in frame (a). Brighter points correspond to larger escape times which are distributed in the interval $[0.18, 1.2]$. (b) Enlargement of a rectangular region of size 0.1 centered at $(0, 0.75)$. (c) Dots represent initial conditions whose escape time is larger than 1.2 in the forward dynamics, and thus form an approximant to the forward nonescaping foliation. (d) Dots represent initial positions whose escape time is larger than 1.2 both in the forward and backward dynamics, and approximate the bounded chaotic set.

call this set the *forward nonescaping foliation*.

One can also construct a similar set corresponding to the time-reversed tracer dynamics starting with the same set of initial conditions. This *backward nonescaping foliation* will exhibit similar patterns.

The intersection of these two foliations has the property that trajectories starting from it never leave the mixing region either in the forward or in the backward dynamics. It is thus a natural generalization of the chaotic saddle introduced in the periodic case, and we call it the *bounded chaotic set*. The most important difference in comparison with periodic flows is that this chaotic set does not contain periodic orbits since the driving flow has an inherently nonperiodic character. It does contain, however, an infinite number of aperiodic bounded orbits. Since nonescaping points in both temporal directions are rather exceptional, we believe that both the nonescaping foliations and the bounded chaotic set are sets of *zero measure*.

We show in Fig. 5(c) the forward nonescaping foliation

obtained by plotting the initial conditions of Fig. 5(a), whose escape times are larger than $t = 1.2$. The filamentary structure is somewhat smeared out due to the low spatial density of the initial conditions considered. Since Eqs. (1) are invariant against the transformation $x \rightarrow -x$; $t \rightarrow -t$, initial positions which are invariant against the transformation $x \rightarrow -x$ lead in the forward and backward dynamics to vortex trajectories mirrored along the $x = 0$ axis. Obviously, this also holds for the advection dynamics. Thus in the case of Fig. 5 the backward nonescaping foliation is simply obtained by mirroring the forward nonescaping foliation against the y axis. The intersection of these foliations, the bounded chaotic set, is shown in Fig. 5(d).

There is another possibility for constructing the bounded chaotic set, namely, by monitoring the evolution of a material line placed in the mixing region. The algorithm is the following: (i) let the vortices move forward in time from $t = 0$ to $t_+ > 0$; (ii) select then a straight material (or dye) line segment in the mixing region and let the vortices move

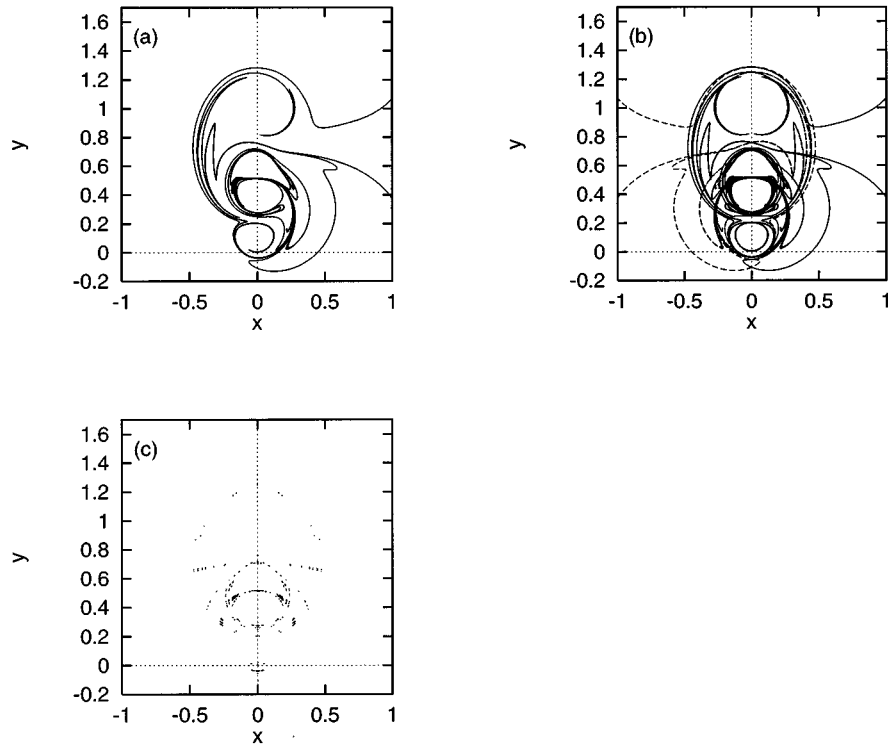


FIG. 6. Approximating the forward and backward nonescaping foliations and their intersections by considering the advection of a material line using the algorithm described in the text. The material line approaching the forward (backward) foliations (full line in (a), (b) [dashed line in (b)]) was at $t=t_+=0.25$ ($t=t_-=-0.25$) a vertical line of length 1.5 centered at $(\pm 1.345, 0.75)$. The intersection of these lines is shown in (c).

backward in time from t_+ to $t=0$ along the same trajectory. Due to the chaotic dynamics, the line evolves to a complicatedly winding curve around the vortices [Fig. 6(a)]. This results in a rapid increase of the length, thus the numerical integration requires more and more interpolating points. Therefore this numerical experiment can only be performed for a relatively short period of time t_+ . Nevertheless the nonescaping points of the winding curve are expected to approach the forward nonescaping foliation as $t_+ \rightarrow \infty$. We can obtain points on the other nonescaping foliation by performing the same procedure but changing the direction of time in (i) and (ii), and replacing t_+ by a $t_- < 0$. The intersection of the two images of the advected material line converges, as the advection times t_+ and t_- go to infinity, to the bounded chaotic set. For simplicity, we can exploit again the above mentioned symmetry of Eqs. (1). Thus the patterns of the material lines in the two cases are mirrored images of each other against the y axis. The intersection [Figs. 6(b) and 6(c)], although obtained from a rather short time evolution of the material lines, shows a structure resembling a double Cantor set, and approximates the bounded chaotic set.

Although the measurement of Fig. 5 provides us with a nice picture of the distribution of escape times in space, its resolution is rather weak. To obtain a higher resolution of the singularities, we followed tracer particles started along a line segment among the vortices and measured the times the particles needed to leave the mixing region. Typical results of such escape-time functions are shown in Fig. 7. This function wildly fluctuates in some regions and has a fine structure of singularities on all scales. This set of singularities corresponds to the intersection of the initial line segment with the

forward nonescaping foliation.

For a quantitative characterization one can measure the decay of tracer particles in the mixing region. Start with an ensemble of N_0 particles and monitor the number $N(t)$ of particles staying still inside after some long enough time t . In the case of periodic flows there is an exponential decay $N(t)/N_0 \sim \exp(-\kappa t)$ characterized by the escape rate κ . In our case the decay is found to be nonuniform (Fig. 8) which means that the escape rate is time dependent. This is again a natural consequence of the chaotic driving of the flow.

One can also observe a nonuniformity of the point density on the value of the escape time (cf. Fig. 7). This can be explained as an effect due to the sharp edge of the mixing region. When a lobe of the droplet ensemble crosses the left edge, there are several initial conditions belonging to nearly the same value of the escape time. For periodic vortex motions, the density differences follow a periodic pattern along the escape-time axis, but now we find a rather irregular density oscillation.

The variation in escape rates implies a nonuniform scaling of the geometry as well. The fractal properties of the singularities of the escape-time function were investigated by the box-counting method. A typical result displayed in Fig. 9(a) shows that the slope on the $\log N(\epsilon)$ vs $\log \epsilon$ plot is not constant. No uniquely defined fractal dimension exists, as can be expected from the variations of the driving present at this scale. In other trials we also found rather accurate scaling from intermediate to small scales [see Fig. 9(b)]. This can be viewed as an effect of the efficient mixing of the different modes present at different scales. The slopes of Fig. 9(b) and Fig. 8(b) (0.95 and 1.3) give an estimate of the

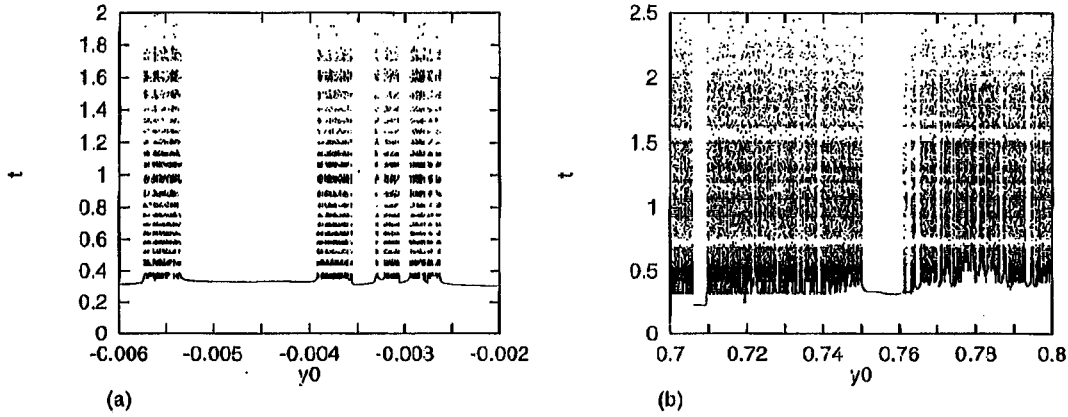


FIG. 7. Escape times t vs initial coordinates y_0 of 100.000 tracer particles. The vortex dynamics corresponds in (a) and (b) to the one represented in Fig. 1(a) and Fig. 1(b), respectively. The particles were started on a vertical line segment centered at (0,0) (a) and (0,0.75) (b).

fractal dimension $d \approx 0.95$ and escape rate $\kappa \approx 1.3 \ln 10 \approx 3.0$. This value of the fractal dimension is in good agreement with the formula $d \approx 1 - \kappa/\lambda \approx 0.945$ [40]. (The average Lyapunov exponent λ is approximated by the slope of the curve presented in Fig. 3: $\lambda \approx 55$.)

IV. RANDOM BAKER MAP MODELS

Observing the motion of a particle advected by a chaotic flow at times $t = n\tau$, i.e., at integer multiples of a time lag τ , defines a sequence of stroboscopic maps connecting the coordinates at $t = n\tau$ with those at $t = (n + 1)\tau$. In contrast to periodic flows, when the map is n independent, it does depend now on the time at which the snapshot is taken. Thus following a trajectory in discrete times requires the application of a sequence of different maps. The actual form of these maps is not known in general *a priori*. If, however, the flow preserves some qualitative features (no drastic changes in the flow structure), the map can be assumed to be an element of a restricted class of maps. Such a class, e.g., can have a given type of dynamics in which only the parameters are n dependent. For sufficiently complex chaotic flows and not very short time lags, the n dependence might be so irregular that subsequent maps correspond to more or less independent choices. This means that on each iterate n , the

map (or the set of its parameters) is randomly taken with respect to a stationary distribution from an ensemble. Such random maps have originally been proposed to understand surface advection generated by temporally chaotic flows in closed containers [36,37,41,42]. The tracer dynamics is then not area conserving due to up and down welling. These maps turned out to be efficient models whose predictions can be compared with experimental observations [10,43].

In the case of the flows investigated here, the preservation of the qualitative features is ensured by the compactness of the configuration of the four vortices maintained in a comoving frame. Therefore the velocity field can be considered at any time as a distorted version of that of two leapfrogging vortex pairs. The random appearance of the flow field can be viewed as a consequence of a projection from the high-dimensional vortex phase space onto a number, the value of the streamfunction at point (x, y) , expressed by Eq. (3) (where the phase space coordinates appear via r_i , $i = 1, \dots, 4$). If the time lag τ is of the order of the dimensionless time unit, the series of $\psi_n(x, y) \equiv \psi(x, y, n\tau)$, or its spatial derivatives which drive the advection process, can be well represented by a random sequence. The new feature in comparison with previous random map models is that we are studying now open incompressible flows, and therefore area

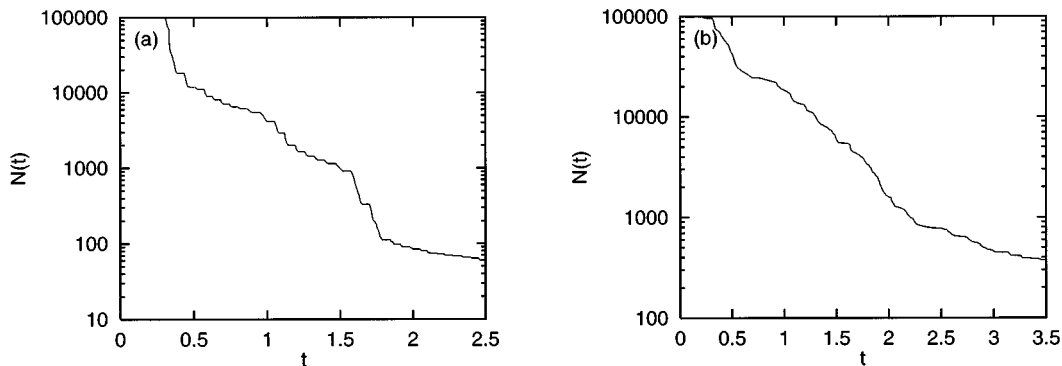


FIG. 8. The number $N(t)$ of particles with escape times larger than t represented as a function of t . (a) and (b) correspond to Figs. 7(a) and 7(b), respectively. A rough estimate of an average escape rate can be read off from the average slopes as $\kappa \approx 1.45 \ln 10 = 3.34$ (a) and $\kappa \approx 1.3 \ln 10 = 3.0$ (b).

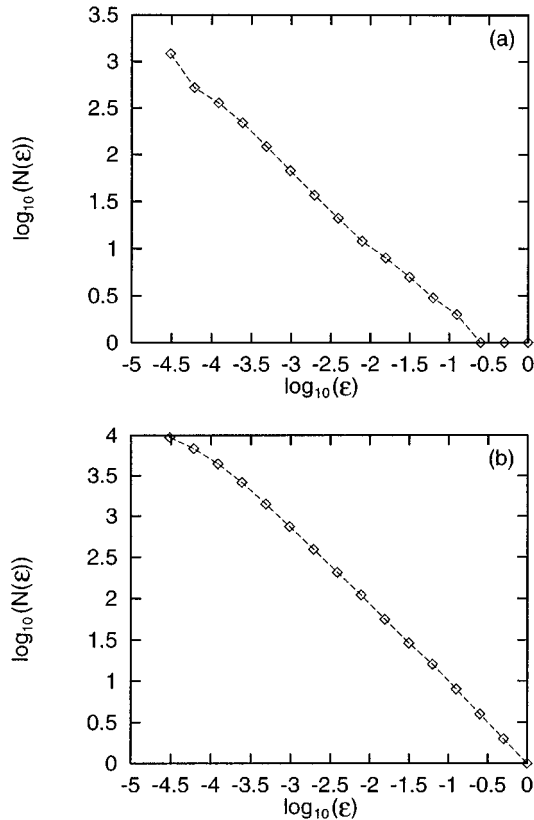


FIG. 9. The number $N(\epsilon)$ of boxes of size ϵ in a box-counting algorithm applied to the set of the initial positions on the line segments shown in Fig. 7, whose escape times are longer than 0.9 (a) and 1.4 (b), respectively. Two local slopes ($d \approx 0.7$ and $d \approx 0.85$) can be read off in (a), while in (b) a well-defined slope gives an estimate of the fractal dimension of the bounded chaotic set (as $d = 0.95$).

preserving open random maps are needed with the possibility of escape.

In this class, perhaps, baker maps are the simplest examples [32]. The simplest deterministic version acts on the unit square by cutting it into two identical horizontal pieces. These strips are squeezed horizontally and stretched vertically so that they become rectangles of size $a \times 1/(2a)$. They are then overlapped with the original square by keeping the two corners fixed (Fig. 10). A repetition of this procedure leads after n steps to 2^n strips of widths a^n inside the square. The squeezing and stretching rates in this process are a and $1/a$, respectively, independently of the construction step. In the asymptotic limit this results in a set of fractal lines of dimension $D = 1 + d$ where the partial dimension d is given by $d = \ln 2 / \ln(1/a)$. The escape rate characterizing the exponential decay of the total area of the strips inside the unit square is simply given by $\kappa = -\ln(2a)$.

Let us now consider a *random* generalization of this process. We make the contraction rates fluctuating by choosing the squeezing rate in step i to be $a_i = a + \delta_i$ with δ_i as a random variable in the range $|\delta_i| \leq \Delta$ with $\Delta < a$ fixed. We assume that the δ_i 's have a *stationary* distribution. The area preservation implies that the expansion rate at step i is $(a_i)^{-1}$. After n steps, we then have 2^n strips of widths $\prod_{i=1}^n a_i$ inside the square. Although the number of strips is

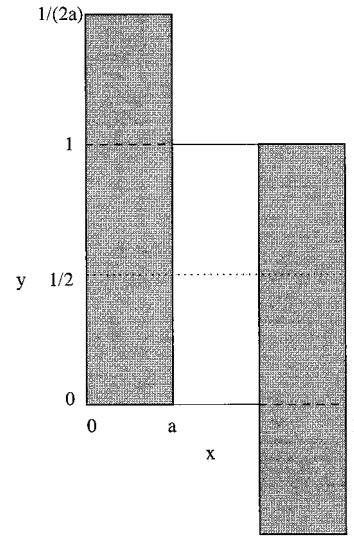


FIG. 10. Schematic representation of an open baker map (see text).

the same as in the deterministic version (the topological entropy is $\ln 2$), no exact self-similar scaling can be found in the length scales. A good numerical approximant to the exact foliation is obtained after $n = 14$ steps. The process illustrates that an ensemble of particles (points on the unit square) subjected to the same noise realization generates a nice foliation, while individual trajectories would trace out a fuzzy pattern only.

By applying a box-counting method along the horizontal direction, one can find that the local slope fluctuates on the $\ln N(\epsilon)$ vs $\ln \epsilon$ plot. One can also plot the time dependence of the total area of the strips inside the unit square (or number of particles N_n) on a logarithmic-linear scale. Fluctuations of the local slope of the $\ln N_n$ vs n curve appear again as an effect of the randomness (cf. Figs. 11, 12). Here we illustrate, by elementary arguments, that although the fluc-

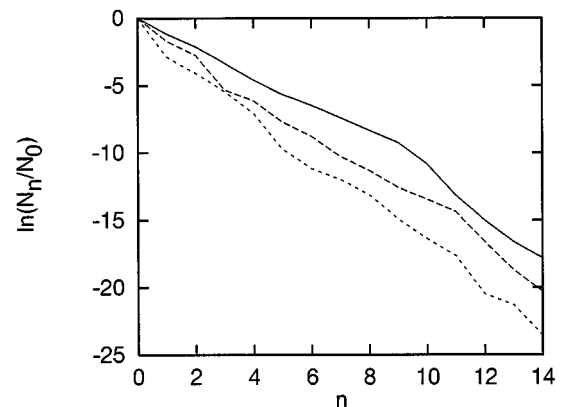


FIG. 11. The total number N_n of particles (inside the unit square) starting with a uniform distribution of N_0 particles (which is proportional to the total area of the strips) as a function of time n . $n_{\max} = 14$ steps were performed with $a_i = a + \delta_i$, where $a = 0.25$ and δ_i is uniformly distributed in the interval $[-0.2, 0.2]$. The results for three different realizations are shown. A well-defined slope will arise after averaging over a great number of realizations.

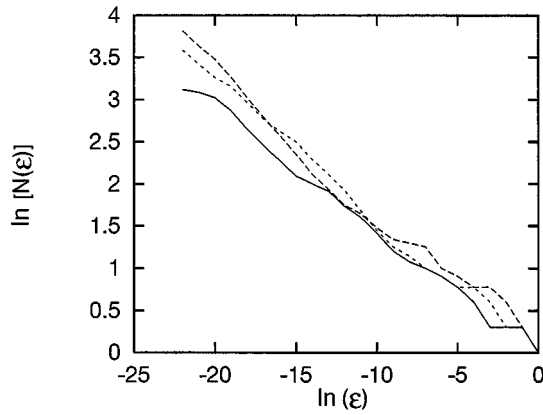


FIG. 12. Number $N(\varepsilon)$ of boxes of size ε needed to cover the projection on the horizontal axis of the strips obtained by a repetition of the random baker map after $n_{\max}=14$ steps, for three realizations of the random sequence δ_i . A well-defined slope will arise after averaging over a great number of realizations. Parameters as in Fig. 11.

tuations are large, a well-defined asymptotic fractal dimension d and escape rate κ exists. This is an extension of the results obtained for the attractors of dissipative and closed random maps [36,37,10].

Let us first investigate the escape rate. We introduce an instantaneous escape rate as $\kappa_i = -\ln(2a_i)$ corresponding to the i th iteration. This would be the value of κ if a_i were independent of i . We define the asymptotic escape rate as

$$\kappa = - \lim_{n \rightarrow \infty} \frac{\ln(N_n/N_0)}{n},$$

where N_n is the number of particles on the square after n steps when starting with a uniform distribution of N_0 particles. Since $N_n/N_0 = 2^n \prod_{i=1}^n a_i$, the average slope of the $\ln N_n$ vs n curve can be written as $[-\sum_{i=1}^n \ln(2a_i)]/n$. Note that for $n \rightarrow \infty$ this yields $\kappa = \langle \kappa_i \rangle$, that is, the average escape rate is simply the average of the instantaneous escape rates (cf. Fig. 11). Note that the average can also be taken over the random process; brackets will be used to denote such averages. Finally we obtain

$$\kappa = \langle \kappa_i \rangle = -\ln 2 - \langle \ln a_i \rangle,$$

i.e., the average of the contraction rates' logarithm determines the escape rate.

The situation is somewhat different for the fractal dimension defined as

$$d = - \lim_{\varepsilon \rightarrow 0} \frac{\ln N(\varepsilon)}{\ln \varepsilon},$$

where $N(\varepsilon)$ is the number of boxes of size ε needed to cover the projection of the foliation on the horizontal axis. Let us consider a box-counting algorithm by choosing a sequence of box sizes ε_n , $n = 1, 2, \dots$ coinciding with the width of the strips after n iterations: $\varepsilon_n = \prod_{i=1}^n a_i$. Since the number of strips is increased by a factor of 2 in each step, the number of nonempty boxes is 2^n in step n . Thus we obtain a set of points on the $\ln N$ vs $\ln \varepsilon$ plot which are equidistant along the

vertical direction. The distance between them along the $y = \ln N(\varepsilon)$ axis is $\Delta y_i = \ln_{10} 2 \equiv \Delta y$. These jumps are, however, distributed unevenly (Fig. 12) along the horizontal $x = \ln \varepsilon$ axis where the distance between successive points is $\Delta x_i = \ln(1/a_i)$. The resulting slope of the $\ln N$ vs $\ln \varepsilon$ curve is $\sum_{i=1}^n \Delta y_i / \sum_{i=1}^n \Delta x_i$ from which

$$\begin{aligned} \frac{1}{d} &= \lim_{n \rightarrow \infty} \frac{1}{n} \sum_{i=1}^n \frac{\Delta y_i}{\Delta x_i} = \lim_{n \rightarrow \infty} \frac{1}{n} \sum \frac{\ln(1/a_i)}{\ln 2} = \left\langle \frac{1}{d_i} \right\rangle \\ &= - \frac{\langle \ln a_i \rangle}{\ln 2}. \end{aligned}$$

This shows that the fractal dimension is equal to the harmonic mean of the local dimensions, $d_i = \ln 2 / \ln(1/a_i)$, which would be the global dimension if a_i was kept independent of i .

By taking into account that $-\langle \ln a_i \rangle$ is the average logarithm of the stretching rate, i.e., the average Lyapunov exponent, we find that $d = 1 - \kappa/\lambda$ holds in this case exactly.

These results can be generalized for the case of nonhomogeneous random baker maps having two different stretching rates a_i and b_i for the two halves of the unit square. In the deterministic case the partial fractal dimension of the resulting nonuniform fractal is given by the implicit equation $a^d + b^d = 1$ [44–46]. If a and b are random variables, one can obtain a successively better and better approximation to the random map's average behavior by applying a sequence of random parameters of length k : $(a_1, b_1), (a_2, b_2), \dots, (a_k, b_k)$, and repeating this sequence periodically up to infinity. After $k=2$ applications of the random map, the widths of the four strips are $a_1 a_2$, $a_1 b_2$, $b_1 a_2$, and $b_1 b_2$. The escape rate κ_2 over this short period is $\kappa_2 = (1/2) \ln(a_1 a_2 + a_1 b_2 + b_1 a_2 + b_1 b_2) = (1/2) [\ln(a_1 + b_1) + \ln(a_2 + b_2)]$. The periodic repetition of this action does not change the escape rate at all, and leads to the construction of a four-scale Cantor set along the horizontal axis. Its fractal dimension is known to be given by the equation [44] $(a_1 a_2)^{d_2} + (a_1 b_2)^{d_2} + (b_1 a_2)^{d_2} + (b_1 b_2)^{d_2} = 1$ which can be rewritten as $(a_1^{d_2} + b_1^{d_2})(a_2^{d_2} + b_2^{d_2}) = 1$. Similarly, for a periodic application of a random sequence of length k we find the escape rate κ_k and partial fractal dimension d_k as $\kappa_k = (1/k) \sum_{i=1}^k \ln(a_i + b_i)$, and $\prod_{i=1}^k (a_i^{d_k} + b_i^{d_k}) = 1$, respectively. The latter can also be written as $\sum_{i=1}^k \ln(a_i^{d_k} + b_i^{d_k}) = 0$. In the limit $k \rightarrow \infty$ we obtain the escape rate κ and partial fractal dimension d of the random map as

$$\kappa = \langle \ln(a_i + b_i) \rangle$$

and

$$\langle \ln(a_i^{d_i} + b_i^{d_i}) \rangle = 0,$$

respectively. Since the order k approximants contain algebraic means of certain combinations of the random parameters, the asymptotic expression appears as mean values taken over the noise realizations. We see again that well-defined dynamical and fractal characteristics exist in open random maps.

The above results can be obtained in a more general setting by using the partition function formalism [37]. In this way, the entire spectrum of the unstable foliation's generalized dimensions [44,45] can also be determined.

V. DISCUSSION

First, let us discuss the relation of the random map approach to chaotically driven advection. We have seen that open random maps possess well-defined asymptotic escape rates and, in spite of their Hamiltonian or area preserving character, also fractal dimensions. The examples clearly demonstrate, however, the difference between the deterministic and random versions. While the exact results for usual baker maps can be read off after one step already, they appear as statistical averages with a $1/n$ type of convergence in random baker maps. This difference remains of course pronounced in more general maps, too, in the form of a much slower convergence in the random version than in the deterministic one.

The effect of noise and chaotic driving is expected to be similar for the properties we are studying. Some differences of course can be pointed out with suitable tailored time series analysis methods [47] but this is not of primary interest for us in this paper. We can state that the escaping process and the tracer foliations in chaotically driven flows are of similar character as in open random (Hamiltonian) maps. This explains the rather large fluctuations of the time decay found in the preceding section since the time interval studied there was yet too short to cover a sampling period where a well-defined average for the escape rate could be obtained. The range of ε used in the box-counting algorithm was much broader, which supports the better scaling found in the $\ln N(\varepsilon)$ vs ε plots.

We do not claim that the simple random baker map studied in Sec. IV would be an appropriate model of advection in the field of chaotically moving vortices in a quantitative sense. Our aim was to show that the existence of an asymptotic escape rate or a fractal dimension is also present in open random maps. Therefore we believe that in sufficiently chaotic flows the long term tracer dynamics can be well modeled by random maps. To find their particular form seems to be rather difficult in practice. Nevertheless, their mere existence is important since it ensures the validity of Kaplan-Yorke type formulas [48] (such as, e.g., a relation $d=1-\kappa/\lambda$ connecting fractality with escape rate and Lyapunov exponent) which can be checked in future experiments (for surface flows in closed domains this has been done in [10]).

There might also be deviations observed from the random map representation. A central assumption has been of course the stationarity of the random process. Since the mixing region is finite, we can assume that such a stationary distribution of the chaotic driving exists and sets in after a finite time. In a particular observation, however, we cannot be sure that the stationarity has already been reached. If this is not the case, no well-defined characteristics can exist, not even

in the weak sense of random averages. The crossover between two more or less linear scaling regimes around $\log_{10} \varepsilon \approx -2.5$ in Fig. 9(a) can be viewed as a consequence of nonstationarity. The vortex trajectories show the succession of two different but more or less periodic vortex motions on the time scales which are relevant for this measurement. The crossover takes place around $x \approx 6.5$ in Fig. 1(a). Thus the two scaling regimes in spatial scales can be considered as fingerprints of these two temporal dynamics.

Recently, the concept of indecomposable continua [29] was introduced and suggested as a useful tool for describing passive advection in open flows. Roughly speaking, an indecomposable continuum is a complicated line that falls into an infinite number of pieces when being cut through by a straight line. This topological property does not imply fractal scaling at all but ensures a geometrical appearance resembling that of fractal manifolds. The forward and backward nonescaping foliations defined in the paper are examples of indecomposable continua. As pointed out, they really do not follow strict fractal scaling but might be characterized by well-defined asymptotic fractal dimensions and escape rates in the sense of open random maps.

Note added: After the submission of this manuscript, we became aware of other recent independent approaches [49–53] devoted to understanding advection in aperiodic flows. In [49] temporally irregular flows are considered. The difference with our paper is that the advection problem investigated is represented there from the very beginning in the form of a random map. Nevertheless the existence of a forward (backward) foliation and a bounded chaotic set (which are called entrainment, pre-entrainment, and intermediate entrainment sets, respectively) is shown, and the corresponding plots of these sets are qualitatively similar to those presented here. The conclusions concerning fractal properties is also similar. Reference [49] contains a detailed study on multifractality, too. Papers [50–53] deal with flows of general time dependence. Rigorous mathematical conditions are worked out for the existence of hyperbolic structures and chaotic sets. In [51] the technique of lobe dynamics and Melnikov's method are generalized for aperiodic flows. In systems with chaotic advection, the above methods and the random map approach seem to be complementary: they provide tools for understanding the short and long time behavior, respectively.

ACKNOWLEDGMENTS

One of us (T.T.) is indebted to Professor A. Provenzale for calling his attention to the relevance of chaotic flows, and for his permanent encouragement. Useful discussions with him, C. Grebogi, G. Haller, H. Lustfeld, O. Piro, and K. G. Szabo are acknowledged. This research was supported by the Hungarian Science Foundation (OTKA Grant Nos. T17493 and T19483) and the U.S.–Hungarian Science and Technology Joint Fund under Project JFNos. 286 and 501. We are thankful to the authors of Refs. [49–53] for sending us their papers prior to publication.

- [1] J. M. Ottino, *The Kinematics of Mixing: Stretching, Chaos and Transport* (Cambridge University Press, Cambridge, England, 1989); J. M. Ottino, *Annu. Rev. Fluid Mech.* **22**, 207 (1990); S. C. Jana, G. Metcalfe, and J. M. Ottino, *J. Fluid Mech.* **269**, 199 (1994).
- [2] H. Aref and N. Pomphrey, *Phys. Lett.* **78A**, 297 (1980).
- [3] H. Aref, *J. Fluid Mech.* **143**, 1 (1984); D. V. Khakhar, H. Rising, and J. M. Ottino, *ibid.* **172**, 419 (1987).
- [4] H. Aref and S. Balachandar, *Phys. Fluids* **29**, 3515 (1986).
- [5] J. Chaiken, R. Chevray, M. Tabor, and Q. M. Tan, *Proc. R. Soc. London, Ser. A* **408**, 165 (1986).
- [6] A. Crisanti *et al.*, *Riv. Nuovo Cimento* **14**, 1 (1991).
- [7] F. J. Muzzio, P. D. Swanson, and J. M. Ottino, *Int. J. Bifurcation Chaos* **2**, 37 (1992).
- [8] S. Wiggins, *Chaotic Transport in Dynamical Systems* (Springer, New York, 1992).
- [9] T. H. Solomon and J. P. Gollub, *Phys. Rev. A* **38**, 6280 (1988); T. H. Solomon, E. R. Weeks, and H. L. Swinney, *Physica D* **76**, 70 (1994).
- [10] J. C. Sommerer and E. Ott, *Science* **259**, 281 (1993); J. C. Sommerer, *Physica D* **76**, 85 (1994).
- [11] R. T. Pierrehumbert, *Chaos Solitons Fractals* **4**, 1091 (1994).
- [12] V. V. Meleshko and G. J. F. van Heijst, *Chaos Solitons Fractals* **4**, 977 (1994); V. V. Meleshko *et al.*, *Phys. Fluids A* **4**, 2779 (1992).
- [13] T. Bohr and J. L. Hansen, *Chaos* **6**, 554 (1994).
- [14] M. Liu, F. J. Muzzio, and R. L. Peskin, *Chaos Solitons Fractals* **4**, 869 (1994).
- [15] G. Boffetta, A. Celani, and P. Franzese, *J. Phys. A* **29**, 3749 (1996).
- [16] Z. Neufeld and T. Tél, *J. Phys. A* **30**, 2263 (1997).
- [17] K. Shariff, A. Leonard, N. J. Zabusky, and J. H. Ferziger, *Fluid Dyn. Res.* **3**, 337 (1988).
- [18] H. Aref, S. W. Jones, S. Mofina, and I. Zawadski, *Physica D* **37**, 423 (1989).
- [19] V. Rom-Kedar, A. Leonard, and S. Wiggins, *J. Fluid Mech.* **214**, 347 (1990).
- [20] K. Shariff, T. H. Pulliam, and J. M. Ottino, *Lect. Notes in Appl. Math.* **28**, 613 (1991).
- [21] K. Shariff and A. Leonard, *Annu. Rev. Fluid Mech.* **24**, 235 (1992).
- [22] C. Jung and E. Ziemniak, *J. Phys. A* **25**, 3929 (1992); C. Jung and E. Ziemniak, in *Fractals in the Natural and Applied Sciences*, edited by M. M. Novak (North-Holland, Amsterdam, 1994); E. Ziemniak and C. Jung, *Phys. Lett. A* **202**, 263 (1995).
- [23] C. Jung, T. Tél, and E. Ziemniak, *Chaos* **3**, 555 (1993); E. Ziemniak, C. Jung, and T. Tél, *Physica D* **76**, 123 (1994); J. B. Weiss, *ibid.* **76**, 230 (1994).
- [24] D. Beigie, A. Leonard, and S. Wiggins, *Chaos Solitons Fractals* **4**, 749 (1994).
- [25] G. Stolovitzky, T. J. Kaper, and L. Sirovich, *Chaos* **5**, 671 (1995).
- [26] Á. Péntek, T. Tél, and Z. Toroczkai, *J. Phys. A* **28**, 2191 (1995); *Fractals* **3**, 33 (1995).
- [27] Á. Péntek, Z. Toroczkai, T. Tél, C. Grebogi, and J. A. Yorke, *Phys. Rev. E* **51**, 4076 (1995).
- [28] J. Kennedy and J. A. Yorke, "The topology of stirred fluids," University of Maryland report, 1995.
- [29] M. A. Sanjuan, J. Kennedy, C. Grebogi, and J. A. Yorke, *Chaos* **7**, 125 (1997); M. A. Sanjuan, J. Kennedy, E. Ott, and J. A. Yorke, *Phys. Rev. Lett.* **78**, 1892 (1997).
- [30] Z. Toroczkai, G. Károlyi, Á. Péntek, T. Tél, C. Grebogi, and J. A. Yorke, *Physica A* **239**, 235 (1997).
- [31] J. C. Sommerer, H.-C. Ku, and H. E. Gilreath, *Phys. Rev. Lett.* **77**, 5055 (1996).
- [32] T. Tél, in *Directions in Chaos*, edited by Hao Bai-Lin (World Scientific, Singapore, 1990), Vol. 3, pp. 149–221; in *STATPHYS'19*, edited by Hao Bailin (World Scientific, Singapore, 1996), pp. 346–362.
- [33] U. Smilansky, in *Chaos and Quantum Physics*, edited by M. J. Giannoni *et al.* (Elsevier, New York, 1992); C. Jung, *Acta Phys. Pol.* **23**, 323 (1992); E. Ott and T. Tél, *Chaos* **3**, 417 (1993); Z. Kovács and L. Wiesenfeld, *Phys. Rev. E* **51**, 5476 (1995).
- [34] D. Elhmaidi, A. Provenzale, and A. Babiano, *J. Fluid Mech.* **257**, 533 (1993); A. Provenzale, A. Babiano, and B. Villone, *Chaos Solitons Fractals* **5**, 2055 (1995).
- [35] A. Babiano, G. Boffetta, A. Provenzale, and A. Vulpiani, *Phys. Fluids* **6**, 2465 (1994); F. Paparella *et al.*, *J. Geophys. Res.* **102**, 6765 (1997).
- [36] E. Ott and T. M. Antonsen, *Phys. Rev. Lett.* **61**, 2839 (1988); *Phys. Rev. A* **39**, 3660 (1989).
- [37] F. Romeiras, C. Grebogi, and E. Ott, *Phys. Rev. A* **41**, 784 (1990).
- [38] P. G. Saffman, *Vortex Dynamics* (Cambridge University Press, Cambridge, England, 1992).
- [39] B. Eckhardt and H. Aref, *Philos. Trans. R. Soc. London, Ser. A* **326**, 655 (1988); B. Eckhardt, *Europhys. Lett.* **5**, 107 (1988).
- [40] H. Kantz and P. Grassberger, *Physica D* **17**, 75 (1985).
- [41] L. Yu, E. Ott, and Q. Chen, *Phys. Rev. Lett.* **65**, 2935 (1990); *Physica D* **53**, 102 (1991).
- [42] A. Namenson, T. M. Antonsen, and E. Ott, *Phys. Fluids* **8**, 2426 (1996).
- [43] J. C. Sommerer, *Phys. Fluids* **8**, 2441 (1996).
- [44] P. Grassberger and I. Procaccia, *Physica D* **13**, 34 (1984).
- [45] T. C. Halsey *et al.*, *Phys. Rev. A* **33**, 1141 (1986).
- [46] T. Vicsek, *Fractal Growth Phenomena* (World Scientific, Singapore, 1992).
- [47] J. Graf von Hardenberg, F. Paparella, N. Platt, A. Provenzale, E. A. Spiegel, and C. Tresser, *Phys. Rev. E* **54**, 394 (1997). J. Graf von Hardenberg, F. Paparella, A. Provenzale, and E. A. Spiegel, in *Nonlinear Signal and Image Analysis*, edited by F. R. Buchler and H. Kandrup (New York Academy of Science, New York, 1997).
- [48] F. Ledrappier and L. S. Young, *Ann. Math.* **122**, 540 (1985).
- [49] J. Jacobs, E. Ott, and T. Antonsen, "Fractal entrainment sets of tracers advected by chaotically temporally irregular fluid flows," University of Maryland report, 1977.
- [50] S. Wiggins, "Chaos in the dynamics generated by sequences of maps, with applications to chaotic advection in flows with aperiodic time dependence," California Institute of Technology, Pasadena report.
- [51] N. Malhotra and S. Wiggins, "Geometric structures, lobe dynamics, and Lagrangian transport in flows with applications to Rossby wave flow, California Institute of Technology, Pasadena report, 1997.
- [52] P. D. Miller, C. K. R. T. Jones, A. M. Rogerson, and L. J. Pratt, "Quantifying transport in numerically generated velocity fields," Brown University report, 1997.
- [53] G. Haller and A. C. Poje, "Finite time transport in aperiodic flows," Brown University report, 1977.